International Journal of ChemTech Research
CODEN (USA): IJCRGG, ISSN: 0974-4290, ISSN(Online):2455-9555
Vol.10 No.3, pp 647-655, 2017

Enhanced electrochemical properties in nanostructured β - MnO_2, synthesized through a single step auto-igniting modified combustion technique.

J.S Sherin[1,3]*, M. Haris[1], D. Shiney Manoj[2], J. Koshy[3] and J.K. Thomas[3]

[1]Department of Physics, Karunya University, Coimbatore, India
[2]Department of Physics, Christian College Kattakada, University of Kerala, Thiruvananthapuram, Kerala, India
[3]Department of Physics, Electronic Materials Research Laboratory, Mar Ivanios college, University of Kerala, Thiruvananthapuram, Kerala, India

Abstract : Nanoparticles of manganese dioxide are prepared by an auto igniting combustion technique and its structural, morphological, optical, and electrochemical properties are investigated. The X-ray diffraction studies reveal that MnO_2 possesses phase pure tetragonal structure with space group of P_{cab}. The average particle size of the as-prepared nanoparticles obtained from both the Scherrer formula and scanning electron microscopy is ~30 nm. EDAX confirms the composition of MnO_2.The UV-vis absorption spectra of the sample was obtained and the optical band gap calculated from Tauc's Plot is 3.25 eV. Electrochemical tests reveal that the sample has a high specific capacitance (320 F/g at 0.25 A/g) and good rate capability, which can be attributed to its unique structure. The capacitance retention reaches 89% after 1000 cycles at a current density of 3 A/g. These results show that manganese dioxide have great potential applications in supercapacitor electrode material.
Keywords : Combustion synthesis,supercapacitor, pseudo-capacitance,charge-discharge process.

1. Introduction

Electrostatic capacitors have been used as energy storage elements for nearly a century, low capacitance values have traditionally limited them to low power applications as components in analogue circuits, or as short-term memory backup supplies. Recent developments in the manufacturing techniques have enhanced the ability to construct materials of high surface-area and electrodes of low resistance having ability to store more energy in the form of electric charge. This has combined with the understanding of the charge transfer processes that occur in electric double-layer to make high-power electrochemical capacitors [1,2]. Electrochemical Double Layer Capacitors (EDLCs), or supercapacitors (SC), are electrochemical capacitors that have high capacitance and high energy density when compared to common capacitors, and high power density when compared to batteries [3]. The mechanisms by which EDLCs store and release charge are completely reversible, hence it is extremely efficient and can withstand a large number of charge/discharge cycles. They can store or release energy very quickly, and can operate over a wide range of temperatures [4].

To achieve high power and high energy density, suitable electrode materials are required to undergo fast reversible redox reactions. Metal oxides (e.g., MnO_2, RuO_2, VO, Fe_2O_3) offer high pseudo capacitance through fast and reversible redox reactions near the surface of active materials. Because of its high specific capacitance (720 F g^{-1}) RuO_2 is one of the most promising candidates for ECs, compared with other less expensive metal oxides such as MO_2 (M = Mn, Pb, Ni) materials. In the past, several attempts are made to explore transition metal oxide materials such as hydrous NiO, MnO_2, Co_3O_4 for high specific capacity supercapacitor applications [5,6]. Manganese oxide among such oxide materials are important because of its attractive high specific capacity, non-toxicity in conjunction with its earth abundance and environmentally compatible. This material had been explored with numerous electrolytes for its pseudo capacitance behaviour where single electron transfer between Mn^{4+} and Mn^{3+} are responsible for the onset of high specific capacitance. Nevertheless, there were ambiguities about the specific capacitance of MnO_2 in different crystalline phases and authors [7]. Zhao et al had reported that specific capacitance is largest in α and δ crystallographic phases ~ 250 F/g and lowest ~ 9 F/g for β crystallographic phase of MnO_2 [8], whereas some recent studies have shown that even nanostructured β-MnO_2 material exhibits better electrochemical performance [9,10].

In the present work, we have synthesized β MnO_2nanopowder using a single step auto igniting combustion technique, and its structural, morphological, optical and electrochemical properties are investigated.

2. Experimental

2.1. Synthesis Procedure.

Manganese sulfate hydrate ($MnSO_4.xH_2O$) dissolved in double distilled water were used as starting reagents from the preparation of nano crystalline MnO_2. Citric acid was then added to the solutions taken in separate beakers as complexing agent. Amount of citric acid was calculated based on the total valance of the oxidising and reducing agents for maximum release of energy during combustion. Oxidant to fuel ratio was adjusted to unity (~1) by adding concentrated ammonium hydroxide solution as a fuel. The precursor solution of P^H ~7.0 was stirred well, for uniform mixing without any precipitation or sedimentation. The solution was then heated using a hot plate kept at ~250^0C in a ventilated fume hood. The solution boils on persistent heating and undergoes dehydration accompanied by foam. On persistent heating the foam gets auto ignited by giving a voluminous fluffy powder of brown MnO_2 nanopowder[15, 16].

In this synthesis procedure, two different concentration of nitric acid carrying 0.3M and 0.7M was added to two replicas of manganese sulfate hydrate solution and 0.6 M was added to a replica of Manganese nitrate hydrated solution. The P^H of the final mixture was found to be 6, 6.5 and 7.5. The solutions were then heated using a hot plate kept at ~250^0C in a ventilated fume hood. The solution boils on persistent heating and undergoes dehydration accompanied by foam. On continuous heating, the foam gets auto ignited by itself giving a voluminous fluffy powder of nano MnO_2 with P^H values 6, 6.5 and 7.5.

2.2 Characterization Technique.

The crystal structure of the prepared particle was determined by X-ray technique using PHILIPS XPERT-PRO diffractometer with nickel filtered CuK_α radiation of wavelength 1.5406 A. Particulate properties of the combustion product were examined using scanning electron microscopy (JEOL Model JSM-6390LV). The UV-Vis spectra of the samples were recorded using JASCO V 570 spectrophotometer in the wavelength range 200 -900 nm. Electrochemical measurements were performed with an Autolab PGSTAT302N. The electrochemical cell had configured with a bright Platinum (Pt) electrode as the counter electrode and the reference electrode used was Ag/Ag Cl electrode. A polished glassy carbon working electrode (GCE) of 5mm in diameter was used a current collector. The working electrodes were prepared by mixing active material with acetylene black and polytetrafluoroethylene (PTFE) with a ratio of 85:10:5. A small amount of 0.5wt% of Nafion solution was added to paste the slurry on the GCE. A 0.5M Na_2SO_4 solution was employed as electrolyte. Cyclic voltammetry (CV) and Galvano static charge –discharge measurements were performed over a potential range from -0.1V to 0.8V at various scan rates (5 to 50 mV/S) and different current densities.

3. Results and Discussion

3.1. X- Ray Diffraction Studies.

The XRD pattern of as prepared MnO_2 nanopowder at different pH through the combustion method is shown in figure 3.1. From the XRD pattern it is evident that MnO_2 crystallizes in single phase and formed stable tetragonal structure. All the peaks including the minor ones are indexed according to the JCPDS file 24-735 for MnO_2 nanoparticles. The strong and intense peaks indicate that the as prepared nanopowders are highly crystalline. No secondary phase or impurity peaks were detected in the pattern and confirms that the phase formation is complete during the combustion process itself, without any calcination. Thus the modified combustion method for the synthesis of nanopowder offers an economic and time saving technique.

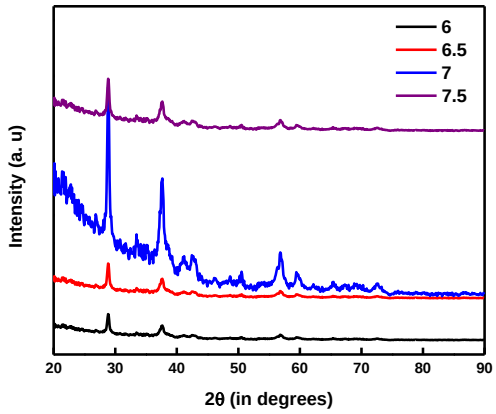

Figure 3.1 XRD pattern of MnO_2 nanoparticle with different pH

The lattice parameters calculated from XRD pattern are well agreeing to the standard reported value. The grain size calculated for MnO_2 nanoparticle using the Scherrer formula ranges from 15 to 26 nm, as pH varies from 6.0-7.5. Based on these results, it is evident that the neutral medium ($P^H \sim 7$) of MnO_2 nanopowder is suitable for preparing materials for magnetic studies, electric as well as electrochemical studies due to the superior nature of the particulate properties of the products. Figure 3.2 shows the Williamson–Hall plot for the as prepared MnO_2 nanopowder. The crystallite size estimate from the plot is 25 nm, and the lattice strain calculated is 0.235. The positive slope shows that the strain is tensile in nature. Even though the lattice strain is very small, it is contributing to the broadening of peaks in the XRD pattern. The Williamson Hall plot for MnO_2 nanopowder obtained at different pH is shown in figure 3.2

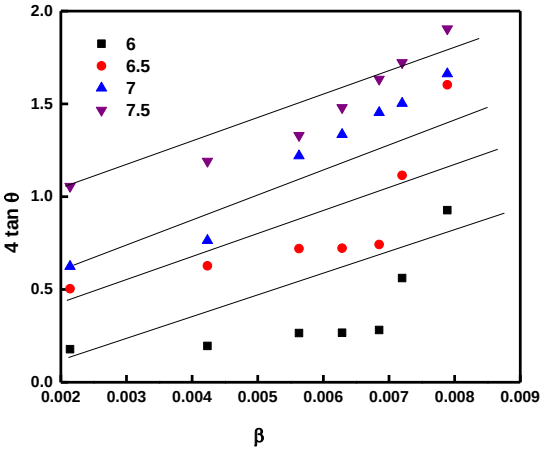

Figure 3.2 W-H plot of MnO_2 nanoparticle

The values obtained for MnO_2 nanoparticles is summarized in the table 3.1

Table 3.1 Lattice parameters, unit cell volume and crystallite size values estimated from the XRD pattern of MnO_2 nanopowder.

pH	Lattice Parameter (Å)				Particle size, D (nm)	Strain, ε		Dislocation density,δ (/m^2)
	Standard		Calculated			Calculated	Graph	
	a	c	a	c				
6	4.399	2.874	5.12	2.47	15	0.2368	0.2364	5.924 X 10^{14}
6.5	4.399	2.874	4.78	2.62	20	0.2359	0.236	3.014 X 10^{14}
7	4.399	2.874	4.39	2.87	25	0.2354	0.2355	1.61 X 10^{14}
7.5	4.399	2.874	4.23	2.98	26	0.2351	0.2352	1.59 X 10^{14}

The XRD pattern of as prepared MnO_2 nanopowder at pH = 7 before and after annealing are shown in the figure 3.3.

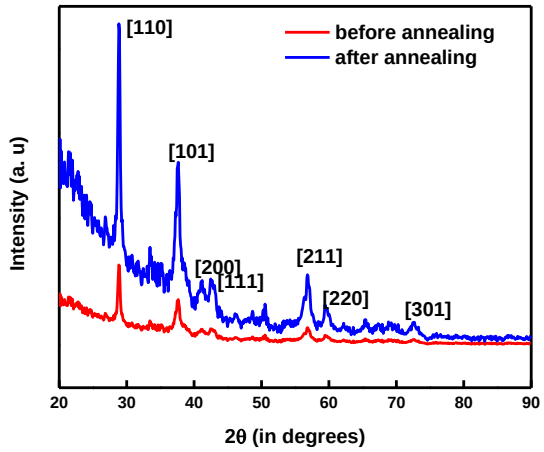

Figure 3.3 XRD pattern of MnO_2 nanoparticle (pH = 7) before and after annealing

3.2 SEM Analysis

The surface morphology and particle size of the samples were revealed using powder SEM micrograph shown in the figure 3.4 of MnO_2 nanoparticles. Both the particles are agglomerated into spherical grains within 20-35 nm range. Each grain results from the agglomeration of smaller particles that are regular in size with rounded edges. The well-defined regions of the nano-grains exhibit definite pores which would contribute immensely to the redox reaction for electrochemical capacitors [10].

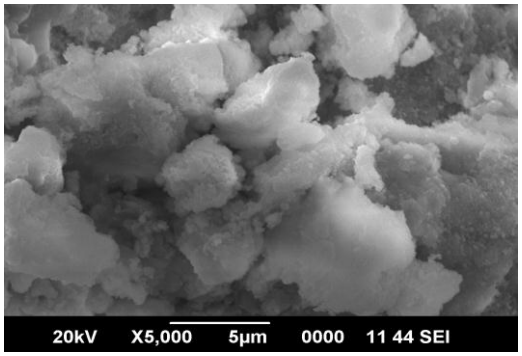

Figure 3.4: SEM of MnO_2 nanoparticle

3.3 EDAX Analysis

The chemical and elemental composition of the as prepared MnO_2 nanoparticles has been examined by subjecting them to energy dispersive X-Ray absorption spectral studies. The EDAX patterns are shown in figure 3.5.

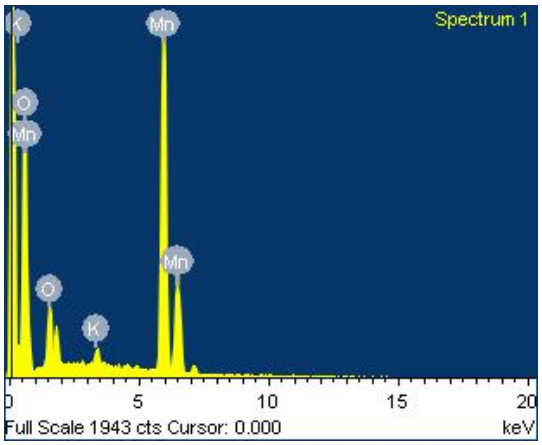

Figure 3.5: EDAX of MnO_2 nanoparticle

Table 3.2: Elemental composition of MnO_2 nanoparticle.

Element	Weight %	Atomic %
O K	38.71	64.00
K K	2.72	2.18
Mn K	58.57	33.82

The EDAX spectrum shows the presence of Mn and O elements in the sample. While the signals of K peaks come from the gridding used for SEM measurement. The composition of elements, weight percentage and atom percentage in each sample are given in table 3.2. The pattern indicates the nanoparticles are composed of manganese and oxygen, shows a high purity of these powders.

3.4 UV- Visible Absorption Spectroscopy

The optical absorption spectra of MnO_2 nanoparticles in the range of 200-900nm at different pH are shown in the figure 3.6

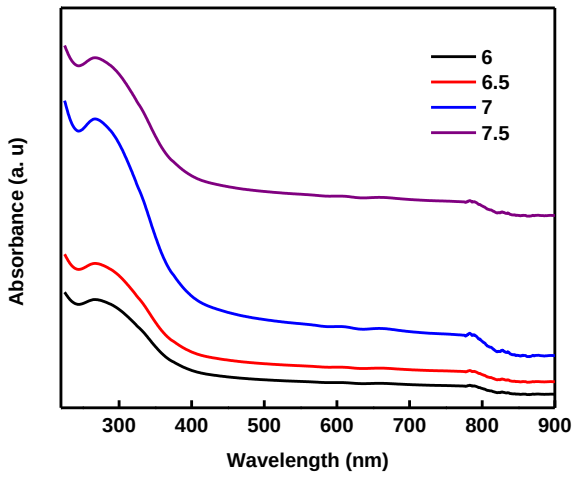

Figure 3.6: UV –Vis spectra of MnO_2 nanoparticle at different pH

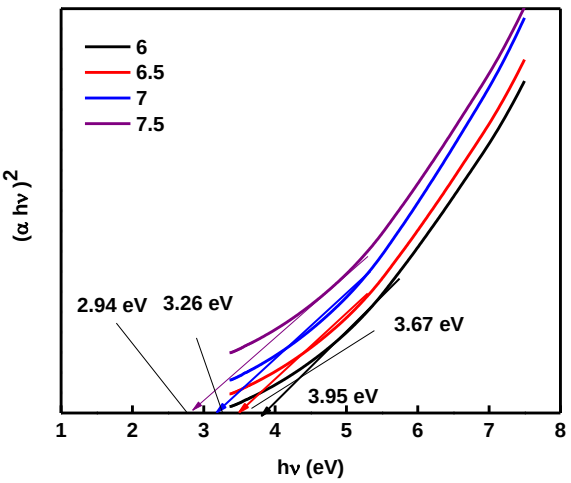

Figure 3.7: Tauc's plot for MnO_2 nanoparticles

Table 3.3: The Bandgap values of MnO_2 at different pH

pH	Bandgap energy,E_g (Calculated)	Bandgap energy, E_g (Tauc's plot)
6	3.85	3.82
6.5	3.69	3.67
7	3.23	3.26
7.5	3.09	2.94

It is clear that the absorbance increased at first and then decreases as the wavelength increases. The spectral observations reveals that both the nanoparticles absorbs photons strongly in the visible region and is highly transparent in the UV region. Based on the above results, we can realise that MnO_2 nanoparticles can be potentially used for devices where the absorption of visible light such as solar cells and photo catalysts are required.

The value of band gap energy (E_g) was estimated by the method proposed by Wood and Tauc, according to the following equation

$(\alpha h\nu)\ \alpha\ (h\nu - E_g)^{n}$

Where E_g is the band gap energy, α is the absorption coefficient, n= ½ for direct transition and n = 2 for indirect transition.

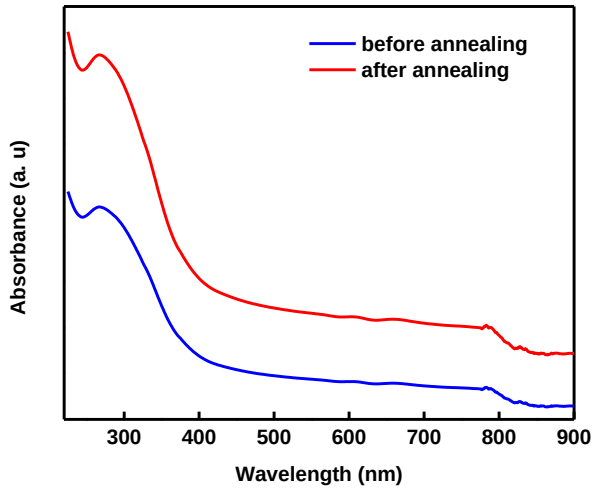

Figure 3.8: UV –Vis spectra of MnO_2 nanoparticle at pH = 7

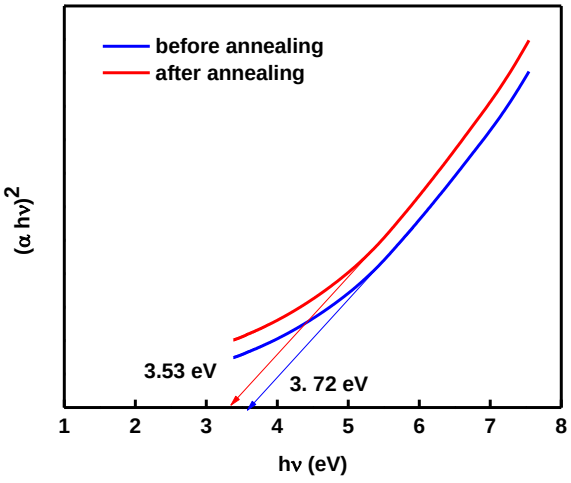

Figure 3.9: Tauc's plot for MnO_2 nanoparticle at pH = 7 before and after annealing

The energy gap values obtained for MnO_2 is 3.26 eV which suggests that the material is a semiconductor. The bandgap values are lower than that reported by Salah. K. Hazza for MnO_2 films [12]. The lowered band gap values may be due to the structural disorder caused by oxygen deficiency in the samples. Thus in order to investigate the effect, the samples are annealed at 450^0C. It is found that the bandgap energy increased after annealing the sample. The obtained values for annealed MnO_2 is 3.63 eV. These values are in good agreement with the reported ones elsewhere for the samples.

3.5 Cyclic Voltammetry.

The capacitive performance of manganese oxides prepared using the present combustion technique is further characterized using cyclic voltammetry. The cyclic voltammograms of manganese dioxide electrodes were measured in 0.5M Na_2SO_4 electrolyte at the scan rates of 100, 50, 25, 10 and 5 mV/s respectively.

The capacitive performance of MnO_2 nanoparticles is evaluated by cyclic voltammetry (CV) techniques in 0.5M Na_2SO_4 solution as shown in figure 3.10A. The measured currents are transformed to gravimetric capacitances by normalizing to electrode mass. Theoretically, an ideal CV curve of an electrochemical capacitor would be of standard rectangular shape since the capacitance C (C=i/mυ where i is the current m is the mass of the active material) would keep constant at a linear charging /discharging rate.

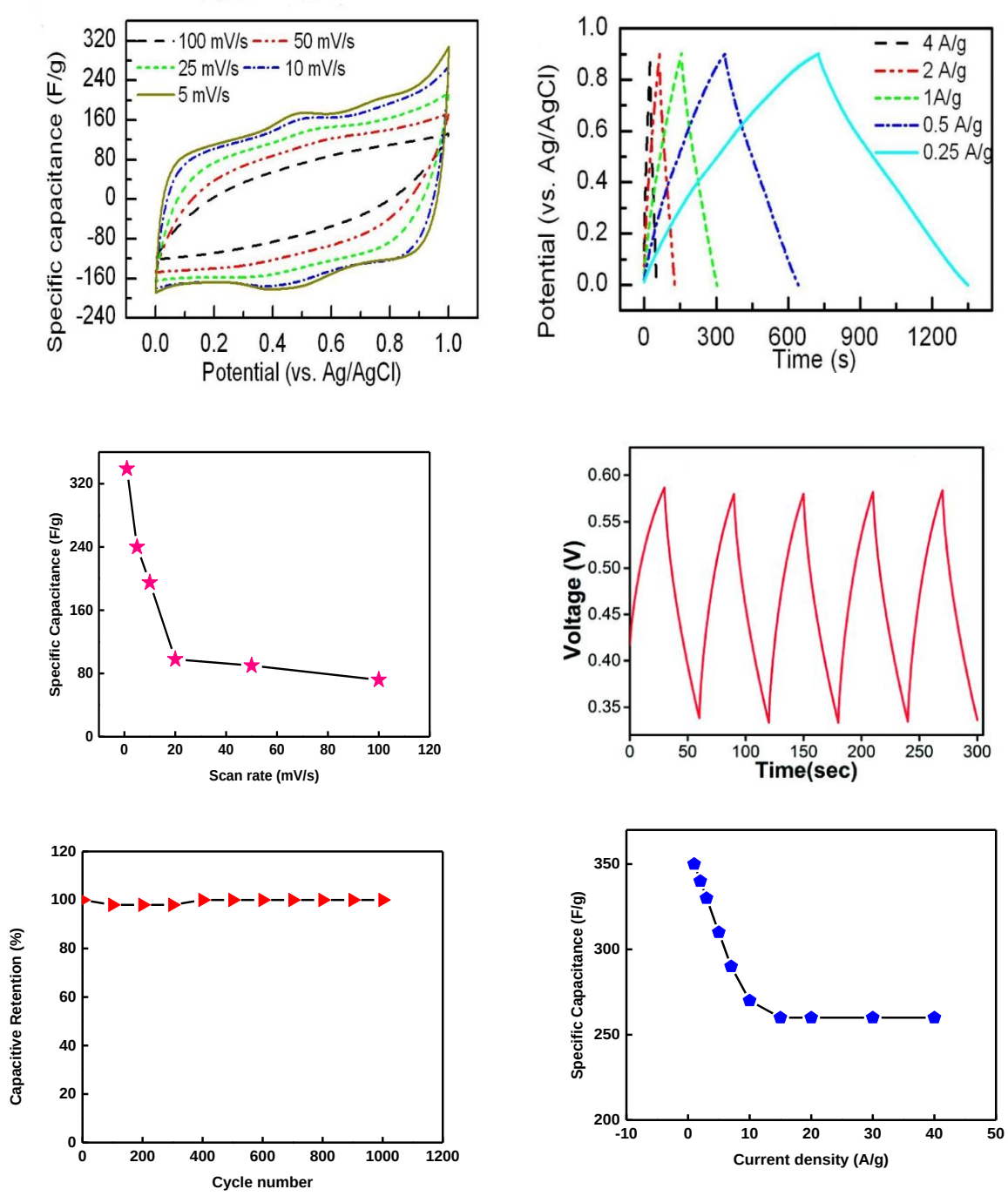

Figure 3.10: (A). CV curve, (B) charge – discharge curve, (C) charge/discharge curves at 0.5A/g, (D) Specific capacitance vs current density, (E) Specific capacitance vs scan rate and (F) Capacitive retention vs cycle number

The figure 3.10A exhibits typical behaviour of the redox reaction of MnO_2 that is rectangular shapes with small redox peaks. The specific capacitance of MnO_2 EC prototype, as determined by integrating the area of CV curve, is substantially larger than the values reported for carbon based systems of similar weight or volume. The capacitance of MnO_2 based EC prototype, arises from rapid and reversible faradaic reactions between electrolyte ions and the electro active material. No redox peaks were discernible from these rectangular CV curves even after prolonged charge/discharge cycling for up to 300 cycles. This could be attributed to the excellent phase stability and reversibility of MnO_2. Taking account of CV curve, it can be inferred that β-MnO_2 exhibited the highest capacitance at a constant scan rate indicating the synergistic effect of MnO_2 nanoparticles. The specific capacitance of MnO_2 was observed to increase substantially from 100 F/g to 310 F/g after 300 charge/discharge cycles. The enhanced electrochemical performance could be attributed to increased surface to volume ratio and accessibility of cations and or protons during charge/discharge cycles.

The charge /discharge curves of β-MnO_2 in figure 3.10B show that the curve exhibits equilateral triangle shapes indicating the good reversibility during the charge/discharge process. However, at the same current density, Na/MnO_2 electrode shows a pronounced potential drop at the beginning of discharge process. The potential drop is attributed to the internal resistance of the electrode associated with resistance in electrical connection, resistance due to the migration of ions in electrode materials. For example, the charge/discharge curves at the current density of 1A/g reveal the IR drop of 0.1V for Na/MnO_2. The IR drop increases linearly with increase of current density. From figure 3.10C the charge/discharge curves of MnO_2 at current density of 0.5 A/g in a potential range of 0 to 0.7V shows, a good linear relation of potential against time that is been regarded as a typical feature of an ideal capacitor.The curves of MnO_2 are symmetric and linear for both charge and discharge portions, indicating that electrodes have good capacitive behaviours with very sharp responses and small internal resistance (IR) drop. The charge curves are symmetric to the corresponding discharge counterparts in the employed potential region, and the slope of the curve is potential independent and maintains a constant value at the selected current density.

The specific capacitance of MnO_2 can be attributed to the fact that the redox process is primarily governed by insertion or extraction of Na^+ from the electrolyte into the nanostructured electrode pores. As the current density increases, the specific capacitance at first increases and then decreases eventually reaches a constant value. The lower values of capacitance at high current rates might be due to less ionic penetration in the electrode surface compared to the case at a low current rate. The capacitance of the cell decreases linearly with increasing current densities, which is the quintessential behaviour of electrochemical supercapacitors, has been found. At low current density, low concentration polarization obstructs the charging process to reach completion with ease and cost effective. Ions in the vicinity of the electrode-electrolyte interface would be enough to improve the redox transitions of manganese oxide, eventually leads to a high capacitance. Hence, the MnO_2 electrode in Na_2SO_4 electrolyte showed a better capacitive performance even at lower current density (Figure 3.10D).

The MnO_2 nanoparticles exhibited a specific capacitance of 330F/g at a scan rate of 2mV/s as shown in figure 3.10E. There is an increase in the specific capacitance when the scan rate at 1 mV/s. Beyond 1 mV/s, the specific capacitance decreases very slowly and shows almost constant at higher scan rate. This shows the electrode is ideal and it can be used for high power applications.To evaluate the long-time cycling stability, the capacitive retention is measured by continuous charge/discharge experiment at a current density of 3.0 A/g. Figure 3.10F shows capacitive retention against cycle number of MnO_2. It is found that the capacitive retentionof the nanomaterialsafter 1000 cycles is about 89% and hence it proved its good cyclic ability. After 1200 cycles, the capacitive retention of the sample is about 75% indicating an acceptable stability. Thus, the capacitance is almost constant with a capacitive retention of about 55% after 1200 cycles.

4.4 Conclusions.

Semiconducting nano – MnO_2 have been synthesized using the modified auto igniting single step combustion process. X-ray diffraction studies showed that the as-prepared nano MnO_2 was single phase with tetragonal having crystalline size in the range of 35-40nm. SEM micrograph of both samples shows spherical morphology and densification of the material with little porosity. The EDAX patterns confirm that the prepared nanopowders have elemental composition of Mn^{4+} and O^{4-} in MnO_2 pattern. The UV- visible study reveals that all the sample absorbs maximum in the UV region. The absorbance spectra show an extension to visible region

in which the materials are ideal for making transparent electrodes and solar cells. The obtained band gap values of the as-prepared samples were 1.64eV which was well agreeing with the reported value which indicated perfect crystalline structure The electrochemical study of manganese dioxide were determined using cyclic voltammetry technique. The CV curve of β- MnO_2 exhibited the highest capacitance at a constant scan rate explains the synergistic effect. The galvanostatic charge/discharge curve shows an equilateral triangle shape indicates the good reversibility. MnO_2 electrode in Na_2SO_4 electrolyte showed a better capacitive performance even at lower current density and also exhibited a specific capacitance of 330F/g at a scan rate of 2mV/s. The cycling ability and capacitive retention of MnO_2 have been studied. About 89% of capacitive retention is possible for β- MnO_2 after 1000 cycles.

Acknowledgements

The authors acknowledge Central Instrumentation Facility, Karunya University, Coimbatore,Electronic Materials Research Laboratory of Mar Ivanios College and Central Instrumentation Centre, Pondicherry Central University, Pondicherry for the facilities provided by them.

References

1. B.E. Conway, Electrochemical supercapacitors: scientific fundamentals and technological applications, Plenum Press, New York, 1999.
2. A. Burke, Journal of Power Sources, 91 (2000) 37-50.
3. P. Simon, Y. Gogotsi, Nature materials, 7 (2008) 845-854.
4. J.R. Miller, P. Simon, Science, 321 (2008) 651-652.
5. M. Inagaki, H. Konno, O. Tanaike, Journal of Power Sources, 195 (2010) 7880-7903.
6. S. Hassan, M. Suzuki, A. Abd El-Moneim, American Journal of Materials Science, 2 (2012) 11-14. 14.
7. K. Hashimoto, M. Yamasaki, K. Fujimura, T. Matsui, K. Izumiya, M. Komori, A. El-Moneim, E. Akiyama, H. Habazaki, N. Kumagai, Materials Science and Engineering: A, 267 (1999) 200-206.
8. X. Zhao, B.M. Sanchez, P.J. Dobson, P.S. Grant, Nanoscale, 3 (2011) 839-855.
9. W. Wei, X. Cui, W. Chen, D.G. Ivey, Chemical Society Reviews, 40 (2011) 1697-1721.
10. L. Xingyou, H. Akihiko, F. Takeshi, C. Mingwei, Nature Nanotechnology, 6 (2011) 232-236.
11. L. Chen, L.J. Sun, F. Luan, Y. Liang, Y. Li, X. X. Liu, Journal of Power Sources, 195 (2010) 3742-3747.
12. Salah.K.Hazaa, Berkala Fisika Indonesi,a 5 (2013)1.
13. F.J. Liu, Journal of Power Sources, 182(2008) 383–388.
14. 14.L.J. Sun, X. X. Liu, European Polymer Journal,44 (2008) 219–224.
15. J. Koshy, J. K. Thomas, J. Kurian, Y. P. Yadava, A. D. Damodaran, U.S. Patent No. 5856276, (1999).
16. J. Koshy, J. K. Thomas, J. Kurian, Y. P. Yadava, A. D. Damodaran, European Patent No. EP 0679615, (1999).
17. 16.A. E. Fischer, K. A. Pettigrew, D. R. Rolison, R. M. Stroud, J. W. Long, NanoLetters,7 (2007) 281–286. 17. C. Qian, H. Qi, B. Gao, Y. Cheng, Q. Qiu, L.C. Qin, O. Zhou, J. Liu, Journal of Nanoscience and Nanotechnology, 6(2006) 1346–1349.
18. 18. P. Staiti, F. Lufrano, Journal of Power Sources,187(2009) 284–289.
19. 19. H.Y. Chen, O. Jacobs, W. Wu, G. Rudiger, B. Schadel, Polymer Testing,26 (2007) 351–360.
20. 20. W. Zhang,M.J Yang, Journal of Material Science, 39 (2009) 4921–4922.
21. 21.A. Zolfaghari, F. Ataherian, M. Ghaemi, A. Gholami, Electrochim. Acta, 52(2007) 2806–2814.
22. 22.D.N. Srivastava, N. Perkas, A. Zaban, A. Gedanken, Pure and Applied Chemistry,74 (2002) 1509–1517.
23. 23.Y. Hou, J. Tang, H.B. Zhang, C. Qian, Y.Y. Feng, J. Liu, ACS Nano,3 (2009), 1057–1062.
24. 24.S.J. Bao, B.L. He, Y.Y. Liang,W.J. Zhou, H. L. Li, Material Science Engineering A,397 (2005) 305–309.
25. 25.M. Chigane, M. Ishikawa, Journal of Electrochemical Society,147 (2000) 2246–2251.
26. 26.M. Chigane, M.Ishikawa, M. Izaki, Journal of Electrochemical Society,148 (2001) D96–D101.
27. 27.M. Toupin, T. Brousse, D. Belanger, Chemistry of Materials, 16(2004) 3184–3190.

*****